Journal of Sound and Vibration (2000) **236**(4), 637–656
doi:10.1006/jsvi.2000.2974, available online at http://www.idealibrary.com on IDEAL®

VIBRATION OF CRACKED CIRCULAR PLATES AT RESONANCE FREQUENCIES

CHI-HUNG HUANG

Department of Mechanical Engineering, Ching Yun Institute of Technology, Chung-Li, Taiwan 320, *Republic of China*

AND

CHIEN-CHING MA

Department of Mechanical Engineering, National Taiwan University, Taipei, Taiwan 106, *Republic of China*

(*Received* 3 *February* 1999, *and in final form* 2 *March* 2000)

It is well known that the presence of cracks will affect the dynamic characteristics of the vibrating plate. Such a problem is complicated because it combines the field of vibration analysis and fracture mechanics. In this study, an optical system called the AF-ESPI method with the out-of-plane displacement measurement is employed to investigate the vibration characteristics of a free circular plate with a radial crack emanating from the edge. The boundary conditions along the circular edge are free. As compared with the film recording and optical reconstruction procedures used for holographic interferometry, the interferometric fringes of AF-ESPI are produced instantly by a video recording system. Based on the fact that clear fringe patterns will appear only at resonant frequencies, both resonant frequencies and corresponding mode shapes can be obtained experimentally at the same time by the proposed AF-ESPI method. Numerical finite element calculations are also performed and the results are compared with the experimental measurements. Good agreements are obtained for both results. The vibrating mode shapes obtained in this study can be classified into two types, symmetric and antisymmetric modes with respect to the crack line. The influence of crack length on resonant frequencies is also investigated in terms of the dimensionless frequency parameter (λ^2) versus crack length ratio (a/D). We find that if the crack face displacement is out of phase, i.e., the antisymmetric type, a large value of stress intensity factor may be induced and the cracked circular plate will be dangerous, from the fracture mechanics point of view. However, there are some resonant frequencies for which the crack face displacements are completely in phase, i.e., the symmetric type, which yields a zero stress intensity factor and the cracked plate will be safe.

1. INTRODUCTION

Holographic interferometry opened new worlds of research by making possible accurate, global measurement of small dynamic surface displacements in a two-step process for a wide variety of objects. For this purpose, different methods of holographic interferometry have been developed for vibration analysis, which have allowed the gathering of a large amount of practical and theoretical information. Unfortunately, the slow and cumbersome process of film development limits the application of holographic vibration analysis in industry. Electronic speckle pattern interferometry (ESPI), which was first proposed by

0022-460X/00/390637 + 20 $35.00/0

Butters and Leendertz [1] to investigate the out-of-plane vibration behavior, is a full-field, non-contact, and real-time measurement technique of deformation for structures subjected to various kinds of loadings. As compared with the traditional holographic interferometry [2], the interferometric fringe patterns of ESPI are recorded by video camera which can eliminate the time-consuming chemical development and speed up the process. Since the interferometric image is recorded and updated at the video camera every $\frac{1}{30}$ s, ESPI is faster in operation and more insensitive to environment than holography. However, this method cannot reach the high image quality of holographic interferometry due to the low resolution of the video camera system. But for practical applications, these disadvantages are outweighed by the high sampling rate of the video camera. Based on the reasons mentioned above, ESPI has become a powerful technique for many academic researches and engineering applications. The most widely used experimental set-up to study dynamic responses by ESPI is the time-averaged vibration ESPI method [3]. The disadvantage of this method is that the interferometric fringes represent the amplitude but not the phase of the vibration. To overcome this shortcoming, the phase-modulation method, using the reference beam modulation technique, was developed to determine the relative phase of displacement [4, 5]. Shellabear and Tyrer [6] used ESPI to make three-dimensional vibration measurements. Three different illumination geometries were constructed, and the orthogonal components of vibration amplitude and mode shape were determined. For the purpose of reducing the noise coming from environment, the subtraction method was developed [7, 8]. The subtraction method differs from the time-averaged method in that the reference frame is recorded before vibration and is continuously subtracted from the incoming frames after vibration. However, the interferometric fringe visibility of the subtraction method is not good enough for quantitative measurement. In order to increase the visibility of the fringe pattern and reduce the environmental noise simultaneously, an amplitude-fluctuation ESPI (AF-ESPI) method was proposed by Wang *et al.* [9] for out-of-plane vibration measurement. In the amplitude-fluctuation ESPI method, the reference frame is recorded in a vibrating state and subtracted from the incoming frame. Consequently, it combines the advantages of the time-averaged and subtraction methods, i.e., good visibility and noise reduction. Ma and Huang [10, 11] used the AF-ESPI method to investigate the three-dimensional vibrations of piezoelectric rectangular parallelepipeds and cylinders, both the resonant frequencies and mode shapes were presented and discussed in detail.

The problem of free vibration of a circular plate was first investigated by Poisson [12] in 1829 and there has been a great amount of subsequent researches and literature [13]. John and Airey [14] proposed a general method for solving the roots of equations involving Bessel functions. From calculating the roots, the radii of nodal circles as well as mode shapes of vibrations were determined for fixed and free circumferential plates. Wah [15] studied the vibration of circular plates with a large initial tension or compression of varying magnitude for the cases of simply supported and clamped edges. According to the Poisson–Kirchhoff theory, the exact solution and numerical results were presented. Eversman and Dodson Jr. [16] treated the problem of the transverse vibration of a centrally clamped spinning circular disk. For different inner/outer radii ratios, the numerical calculation was carried out from zero to two nodal diameters and from zero to two nodal circles. Itao and Crandall [17] tabulated the natural modes and natural frequencies for the first 701 modes of an isotropic thin circular plate with a free edge. However, the natural frequencies which were calculated based on the classical plate theory could not be determined accurately for the higher modes. Taking account of both rotatory inertia and shear deformation of the plates, Irie *et al.* [18] employed the Mindlin plate theory to obtain more accurate results. Stavsky and Loewy [19] considered the axisymmetric vibration of

isotropic composite circular plates with clamped edges. Combining the transcendental frequency equation with the characteristics cubic equation, the frequency variation versus layer thickness could be obtained and examples of steel–aluminum composite plates were presented. Marchand *et al.* [20] used free vibration of plates to determine the material constants for a circular ceramic plate on the basis of the Mindlin plate theory. There are approximately 200 technical publications accumulated in the literature [21–23] for the free vibration characteristics of complete circular and annular plate with various support conditions along the circumferential boundaries. Leissa *et al.* [24] studied the vibration behavior for completely free circular plates with V-notches. Due to the bending moment singularities, the theoretical analysis included two sets of admissible functions, algebraic-trigonometric polynomials and corner functions, to enhance the convergence and represent the corner singularity. The non-dimensional frequency parameters of plates for various notch angles and depths were investigated by means of numerical calculations and some mode shapes were also presented. Besides, the problem of plates with radial cracks was included when the notch angles approach zero. McGee *et al.* [25] employed a similar method, as mentioned above, to investigate the free vibration for thin circular plates with clamped V-notches. Ramesh *et al.* [26] considered the vibration of an annular plate with periodic radial cracks and investigated the influences of the number and length of cracks on natural frequencies. Both the rap and shaker table tests were performed and the modes were classified according to the number of nodal diameters and nodal circles. However, there are very few experimental results, especially for the full-field measurement of mode shapes, available in the literature.

The study of the vibration behavior of a plate with cracks is a problem of great practical interest. It is known that the presence of cracks will affect the dynamic characteristics of the plates for both resonant frequencies and mode shapes. Such a problem is complicated because it combines the field of vibration analysis and fracture mechanics. Only a few papers have been published on the vibration analysis of finite cracked plate. In this paper, the optical method based on the amplitude-fluctuation ESPI (AF-ESPI) is employed to study experimentally the resonant characteristics of free vibration circular plates with radial cracks. The boundary conditions along the circular edge are free. The advantage of using AF-ESPI method is that both resonant frequencies and the corresponding mode shapes can be obtained simultaneously from the experimental investigation. This is a great aid to our study of the influence of the crack length on the vibration behavior. In addition to the AF-ESPI experimental technique, numerical computations based on a finite element package are also presented and good agreements of resonant frequencies and mode shapes are found for both results. Furthermore, crack face opening displacements are calculated to study the fracture problem induced by the resonant vibration. It is interesting to find that at some resonant frequencies the crack face displacements are symmetric modes, which causes a zero stress intensity factor, and the cracked plate will be safe from the fracture mechanics point of view.

2. OPTICAL AF-ESPI METHOD FOR VIBRATION MEASUREMENT

The optical arrangement of ESPI method for out-of-plane vibrating measurement is shown schematically in Figure 1. If the image of the specimen is taken at the stress-free state, the light intensity detected by a CCD camera can be expressed by the time-averaged method as

$$I_0 = \frac{1}{\tau}\int_0^{\tau} (I_A + I_B + 2\sqrt{I_A I_B}\cos\phi)\,\mathrm{d}t = I_A + I_B + 2\sqrt{I_A I_B}\cos\phi, \tag{1}$$

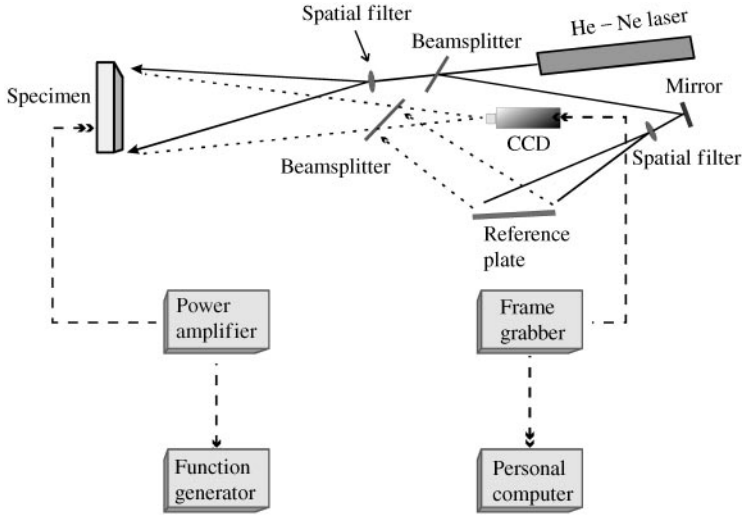

Figure 1. Schematic diagram of the ESPI set-up for out-of-plane displacement measurement.

where I_A is the object light intensity, I_B the reference light intensity, τ the CCD refreshing time, and ϕ the phase difference between object and reference light.

Assuming that the specimen vibrates at a resonant frequency, then the light intensity taken by the CCD camera can be represented as

$$I_1 = \frac{1}{\tau}\int_0^{\tau}\left\{I_A + I_B + 2\sqrt{I_A I_B}\cos\left[\phi + \frac{2\pi}{\lambda}(1+\cos\theta)A\cos\omega t\right]\right\}\mathrm{d}t, \tag{2}$$

where λ is the wavelength of laser, θ the angle between object light and observation direction, A the vibration amplitude, and ω the angular frequency.

Let $\Gamma = (2\pi/\lambda)(1+\cos\theta)$ and assume that $\tau = 2m\pi/\omega$, where m is an integer; then equation (2) can be expressed as

$$I_1 = I_A + I_B + 2\sqrt{I_A I_B}\,(\cos\phi)\mathrm{J}_0(\Gamma A), \tag{3}$$

where J_0 is a zero-order Bessel function of the first kind. When these two images (I_0 and I_1) are subtracted and rectified by the image processing system, i.e., subtracting equation (1) from equation (3), the resulting image intensity can be expressed as

$$I = I_1 - I_0 = 2\sqrt{I_A I_B}\,|(\cos\phi)[\mathrm{J}_0(\Gamma A) - 1]|. \tag{4}$$

The expression of light intensity of the image shown in equation (4) is called the subtraction method, and the reference image is recorded before loading is applied.

Instead of using the subtraction method, the AF-ESPI method is employed in this study by taking two images after the specimen vibrates and assuming that the vibration amplitude of the second image has changed from A to $A + \Delta A$. The light intensity of the second image will be

$$I_2 = \frac{1}{\tau}\int_0^{\tau} I_A + I_B + 2\sqrt{I_A I_B}\cos[\phi + \Gamma(A+\Delta A)\cos\omega t]\,\mathrm{d}t. \tag{5}$$

Expanding equation (5) by using Taylor series and neglecting higher order terms, we have

$$I_2 = I_A + I_B + 2\sqrt{I_A I_B}\,(\cos\phi)[1 - \tfrac{1}{4}\Gamma^2(\Delta A)^2]\mathrm{J}_0(\Gamma A). \tag{6}$$

When these two images (I_1 and I_2) are subtracted and rectified by the image processing system, i.e., subtracting equation (3) from equation (6), the resulting image intensity can be expressed as

$$I = I_2 - I_1 = \frac{\sqrt{I_A I_B}}{2}\,|(\cos\phi)\Gamma^2(\Delta A)^2\mathrm{J}_0(\Gamma A)|. \tag{7}$$

Compared with the subtraction method, the reference image is recorded and subtracted at the vibrating state by the AF-ESPI method. As indicated in equations (4) and (7), the dominant function of the AF-ESPI method is $|\mathrm{J}_0(\Gamma A)|$ and that of the subtraction method is $|\mathrm{J}_0(\Gamma A) - 1|$. Owing to the discrepancy between the dominant functions, the nodal lines of vibrating interferometric patterns obtained by the AF-ESPI method are the brightness lines and those by the subtraction method are the darkness lines. These characteristics of the AF-ESPI method can be used as a qualitative observation or quantitative analysis for the fringe patterns. Furthermore, the sensitivity and fringe visibility of the AF-ESPI method are better than these of the subtraction method. It can be verified that the number of fringes presented by the AF-ESPI method is about twice that by the subtraction method under the assumption of same vibration amplitude. In addition to the theory of out-of-plane measurement mentioned above, the in-plane vibration measurement by the AF-ESPI method can also be derived in a similar way [11].

3. EXPERIMENTAL RESULTS AND NUMERICAL ANALYSIS FOR CRACKED CIRCULAR PLATES

An aluminum circular plate (6061T6) with a radial crack emanating from the edge is used in this study for experimental investigations and numerical calculations, the material properties of the cracked plate are mass density $\rho = 2700\ \mathrm{kg/m^3}$, Young's modulus $E = 70$ Gpa and the Poisson ratio $\nu = 0{\cdot}33$. The geometric dimensions of the cracked circular plate are shown in Figure 2 where the crack length a is taken to be 10, 20, 30, 40 and 50 mm in the analysis. The boundary conditions along the circular edge are free. A self-arranged AF-ESPI optical system as shown in Figure 1 is employed to perform the out-of-plane vibration measurement for the resonant frequency and the corresponding mode shape. As shown in Figure 1, a 30 mW He–Ne laser with wavelength $\lambda = 632{\cdot}8$ nm is used as the coherent light source. The laser beams is divided into two parts, the reference and object beams, by a beamsplitter. The object beam travels to the specimen and then reflects to the CCD camera (Pulnix company). The reference beam is directed to the CCD camera via a mirror and the reference plate. It is important to note that the optical path and the light intensity of these two beams should maintain identically in the experimental set-up. In order to increase the intensity of light reflection of specimens and the contrast of fringe patterns, the surfaces of plates are coated with white paint which is mixed with fine seaweed powder. The cracked circular plate is excited by a piezostack actuator (PI company) which is attached behind the specimen, and the specimen is placed on a sponge to simulate the traction-free boundary condition. To achieve the sinusoidal output, a function generator HP33120A (Hewlett Packard) connected to a power amplifier (NF corporation) is used. Numerical results of resonant frequencies and mode shapes are calculated by ABAQUS

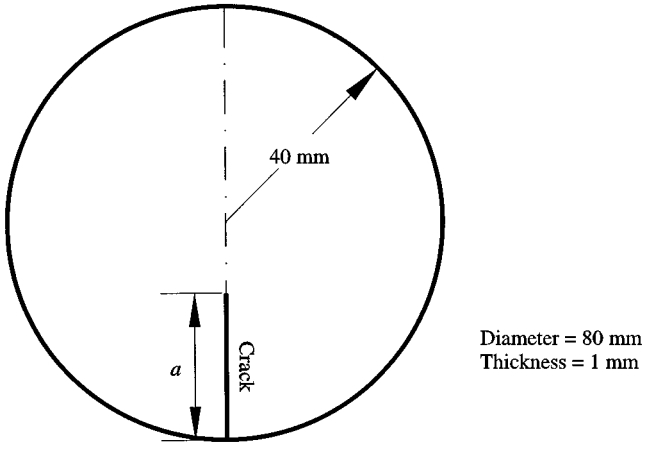

Figure 2. Geometric dimension and configuration of the cracked circular plate.

finite element package [27] in which eight-node two-dimensional shell elements (S8R5) are selected to analyze the problem. By placing the first node near the crack tip away from the regular position at one quarter of the distance to the second point, named "quarter-point" method, the square root singularity will be manipulated near the crack tip.

Table 1 shows the experimental and numerical results of resonant frequencies of the first 10 modes for cracked circular plates with different crack lengths. We can see that these two results are quite consistent. For convenience, we note that C10 represents the circular plate with crack length 10 mm and C0 is the circular plate without crack. The theoretical results of the resonant frequencies are available for the C0 plate and are included in Table 1 to validate the FEM results. The analytical results of the first six resonant frequencies obtained by Leissa *et al.* [24, Table 4] for C10, C20 and C40 plates are also represented in Table 1. The difference between the results obtained by Leissa *et al.* [24] and the FEM is about 1 per cent. Since the weight of the specimen increases slightly by the attached actuator, the resonant frequencies obtained from experimental measurement turn out to be lower than the numerical results. For conciseness, only experimental results of mode shapes for circular plate without crack, with short crack (crack length 20 mm) and long crack (crack length 50 mm) are presented. Figures 3–5 are the first 10 mode shapes for both experimental measurements and numerical simulations. For the finite element calculations, the contours of constant displacement for resonant mode shapes are plotted in order to compare with the experimental observation. In Figures 3–5, we indicate the phase of displacement in finite element results as " + " or " − " sign, the regions of the same sign represent the motion in phase and nodal lines are located between " + " and " − " signs. The brightest fringes on experimental results represent the nodal lines of the vibrating cracked plate at resonant frequencies. The rest of the fringes for AF-ESPI are contours of constant amplitudes of displacement. A good agreement is found between the experimental and numerical results for both the resonant frequencies and the mode shapes.

In order to discuss the influence of the crack length on the resonant frequency, the resonant frequency f is expressed in terms of a non-dimensional frequency parameter λ^2 given by

$$\lambda^2 = 2\pi f\left(\frac{D}{2}\right)^2\sqrt{\frac{12\rho(1-\nu^2)}{Eh^2}},$$

TABLE 1

First 10 *resonant frequencies obtained from AF-ESPI and FEM for cracked circular plates*

Mode	C0			C10		C20		C30		C40		C50	
	AF-ESPI (Hz)	FEM (Hz)	Theory (Hz)	AF-ESPI (Hz)	FEM (Hz)	AF-ESPI (Hz)	FEM (Hz)	AF-ESPI (Hz)	FEM (Hz)	AF-ESPI (Hz)	FEM (Hz)	AF-ESPI (Hz)	FEM (Hz)
1	792	814	815	784*	802* (811*)	716*	734* (743*)	563*	576*	407*	417* (423*)	297*	306*
2	1374	1400	1405	788	803 (811)	748	768 (777)	703	714	627	646 (656)	553	569
3	1805	1893	1896	1361	1397 (1375)	1348	1361 (1343)	1206	1243	1130	1158 (1170)	1095	1121
4	3110	3171	3177	1785*	1838* (1855*)	1490*	1522* (1543*)	1241*	1279*	1162*	1187* (1183*)	1102*	1124*
5	3240	3327	3334	1818	1848 (1865)	1723	1766 (1783)	1692	1728	1665	1725 (1732)	1678	1718
6	4965	5112	5121	3054*	3119* (3105*)	2467*	2540* (2564*)	2295*	2352*	2187*	2251* (2272*)	1812*	1868*
7	5326	5436	5458	3092	3149	2906	2975	2765	2843	2619*	2697*	2331*	2403*
8	5780	5922	5965	3150*	3208*	3085*	3172*	3021*	3104*	2738	2802	2733	2799
9	7035	7250	7156	3200	3240	3148	3219	3142	3213	3105	3203	3108	3201
10	7910	8154	8195	4632*	4725*	3937*	3982*	3752*	3824*	3562*	3677*	3551*	3657*

*represents the antisymmetric types, and ( ) represents the data taken from Leissa *et al.* [24].

where D is the diameter and h is the thickness of the cracked circular plate. Figure 6 shows the dependence of resonant frequency (λ^2) on non-dimensional crack length (a/D) for cracked circular plates. As expected from the fact that the stiffness of the cracked plate decreases as the crack length increases, all the resonant frequencies decrease with increasing

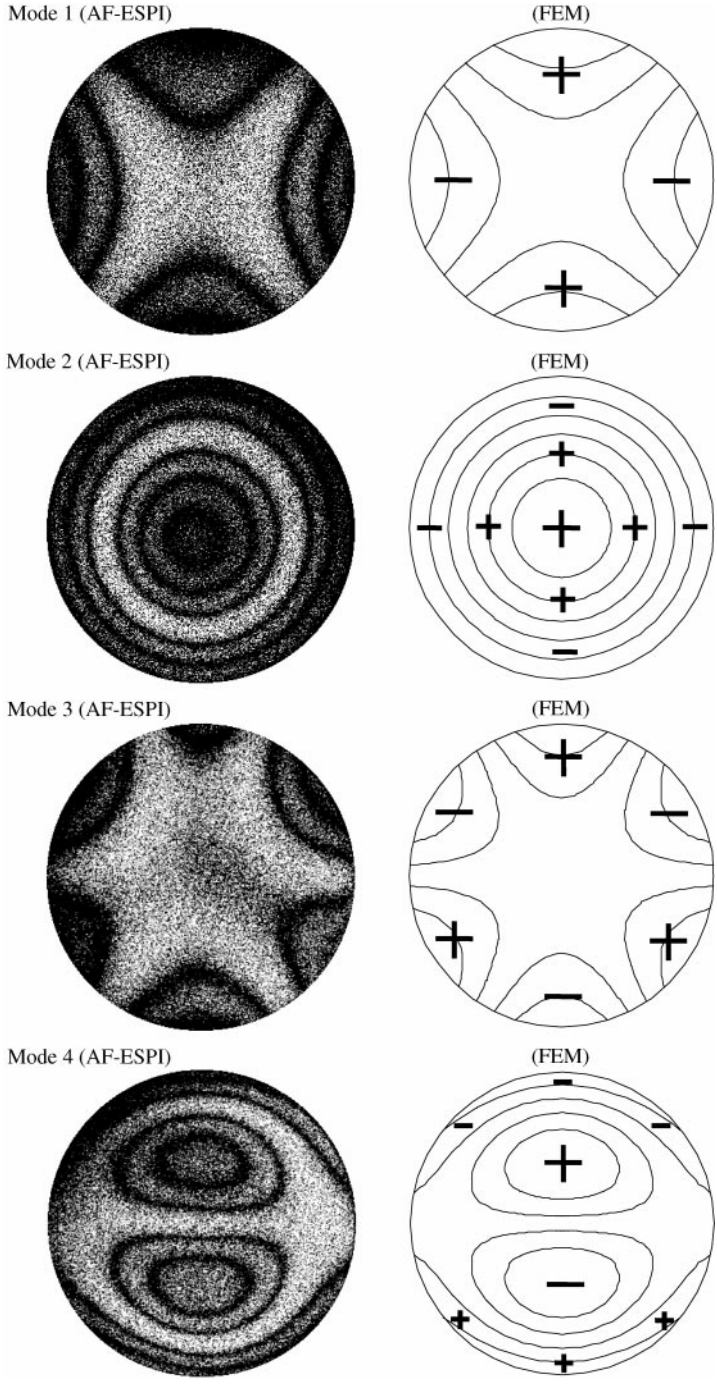

Figure 3. Mode shapes of the circular plate without crack obtained by AF-ESPI and FEM.

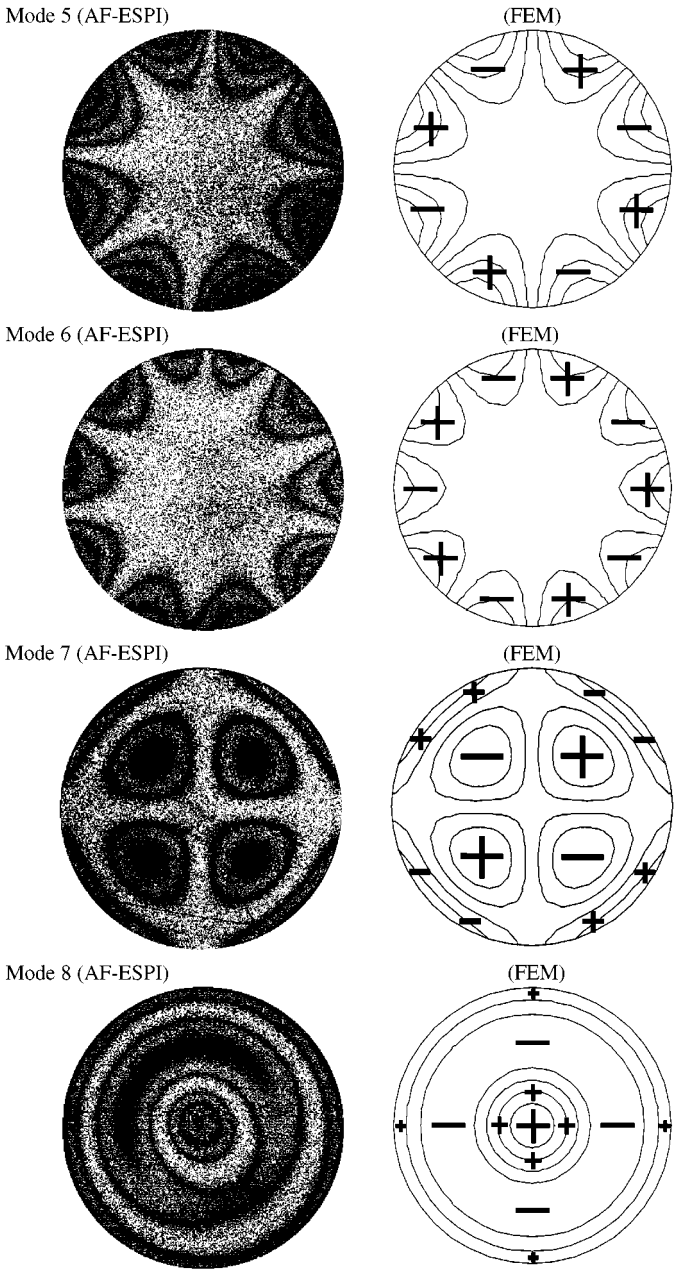

Figure 3. Continued.

crack length. We can find in Figure 6 that the frequencies decrease drastically for modes 1, 4, 6 and 10 which correspond to the pure antisymmetric type of mode shape as indicated in Table 1. An anti-symmetric mode means that the displacements are out of phase for two regions divided by the central line along the crack. For pure symmetric types, such as modes 2, 3, 5 and 9, the resonant frequencies show only a slight dependence on the crack length. It is worth noting that symmetric types almost maintain similar mode shapes for different crack lengths as shown in Figures 4 and 5. However, it is interesting to indicate that modes

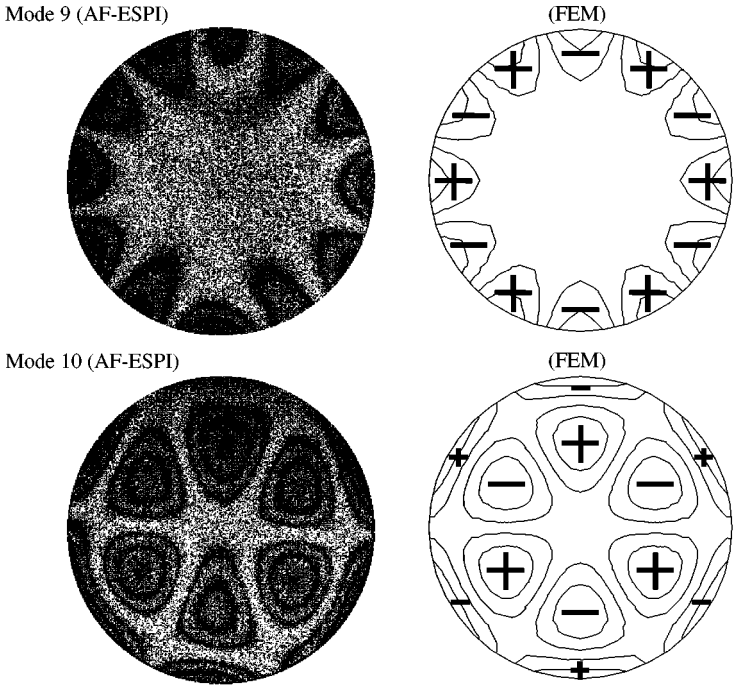

Figure 3. Continued.

7 and 8 change the characteristics of mode shapes from symmetric (antisymmetric) type to antisymmetric (symmetric) type as the crack length increases, and we call it the mixed type. The variation of resonant frequencies for mixed type will lie between the pure antisymmetric and symmetric cases as mentioned above.

Finally, the crack face displacement and the crack opening displacement (COD) for different resonant frequencies and crack lengths of the cracked circular plates are investigated and the results are shown in Figures 7 and 8. In these figures, the out-of-plane displacement w and COD along the crack face are normalized with w_{max} which is the maximum displacement in the whole plate, the distance from the crack face to the crack tip is denoted as x and is normalized with the crack length a. From a fracture mechanics point of view, the out-of-plane displacement will induce a mode III (antiplane mode) type of fracture problem. A large value of COD will induce a large stress intensity factor which will initiate crack propagation and the cracked plate will be dangerous. Figures 7(a) and 7(b) show the crack face displacement of the C20 plate for 10 modes; there are five modes (modes 2, 3, 5, 7 and 9) that the two crack faces are completely in phase, and five modes (modes 1, 4, 6, 8 and 10) are out of phase. Figure 7(c) shows the result of the crack opening displacement (i.e., the difference of the displacement between upper and lower crack faces) for the C20 plate. We can see that if the crack face displacements are in phase then the COD will be zero and the COD varies almost linearly along the crack face for the case of out of phase. For long crack, i.e., C50 plate, the results are shown in Figures 8(a)–8(c). There are also five modes (modes 2, 3, 5, 8 and 9) in phase and five modes (modes 1, 4, 6, 7 and 10) out of phase, and the COD is zero for the case of in phase. It is also indicated that if the displacement is zero at some points in the crack face, then the nodal line will intersect with that point. This phenomenon can be illustrated by experimental results in Figures 4 and 5. It is worth noting that if the displacement of crack faces is out of phase, then the crack tip is always located at

the nodal line. Note that for the C50 plate the crack faces cross each other for modes 6, 7 and 10 at about $x/a = 0{\cdot}9$, $0{\cdot}6$ and $0{\cdot}16$ respectively. From fracture mechanics point of view, the dangerous cases are modes 1, 4, and 6 since they have large values of COD. It is concluded that the COD is zero when the displacement of crack faces is in phase (i.e., modes 2, 3, 5, 7 and 9 for the C20 plate and modes 2, 3, 5, 8 and 9 for the C50 plate) and the stress intensity factor will be zero, which implies that the crack will not propagate in these resonant frequencies for the cracked circular plate.

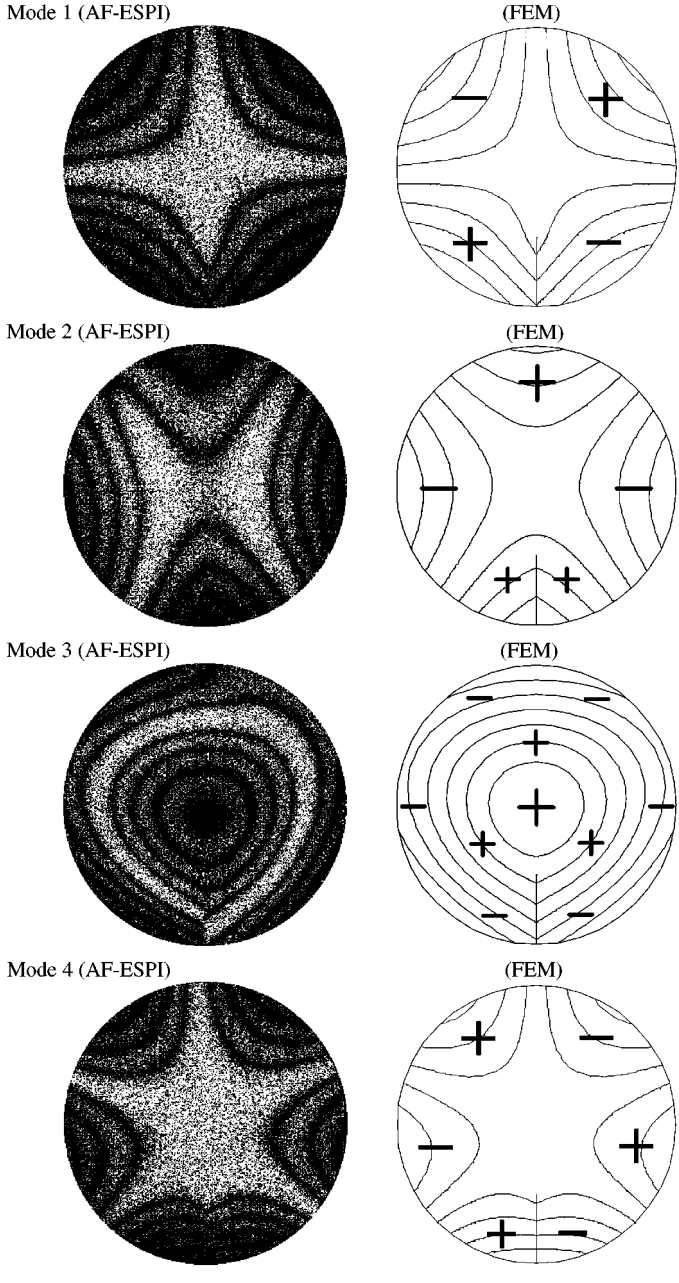

Figure 4. Mode shapes of the C20 plate obtained by AF-ESPI and FEM.

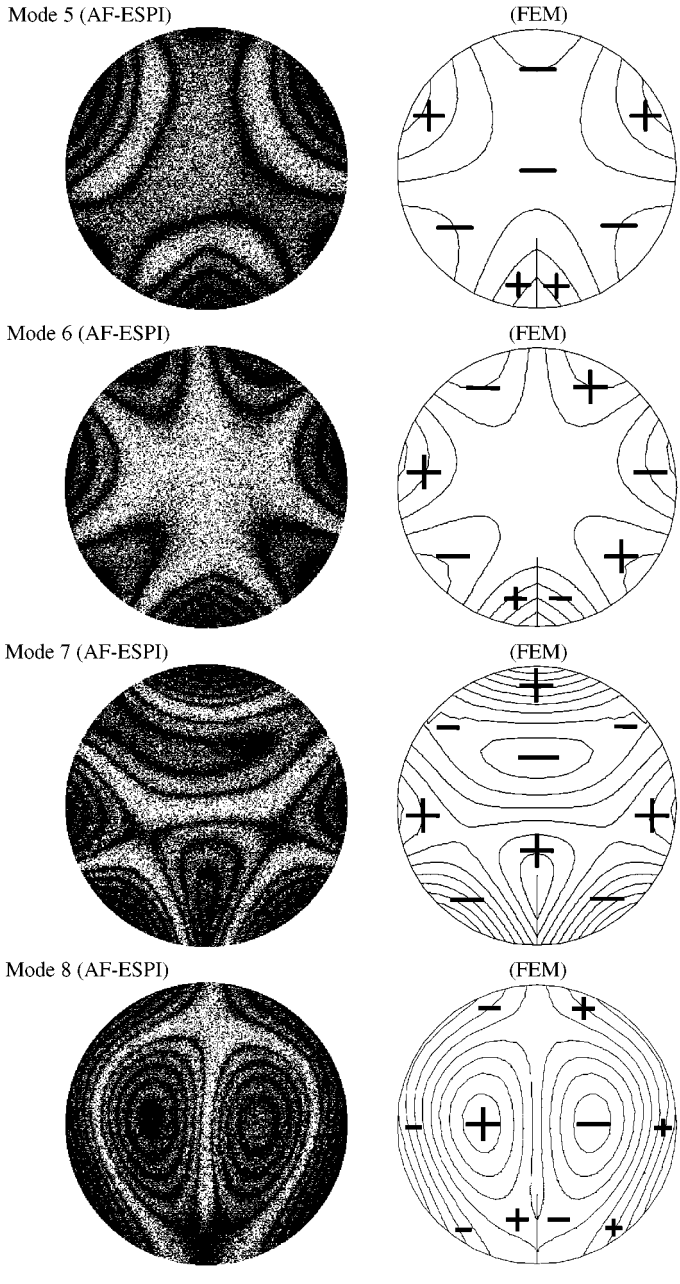

Figure 4. Continued.

Because the existence of a crack will destroy the axisymmetric characteristics and introduce a new free boundary of the circular plate, the nodal lines of the cracked circular plate are no longer simply composed of diameters and circles as in the case of a circular plate without crack. It is interesting to note that resonant mode shapes of the symmetric types for the cracked circular plate are safe from the fracture mechanics point of view due to the zero COD value. Consequently, the cracked plate will be dangerous for those resonant frequencies in which the crack face displacement is out of phase, i.e., the mode shape is of the antisymmetric type.

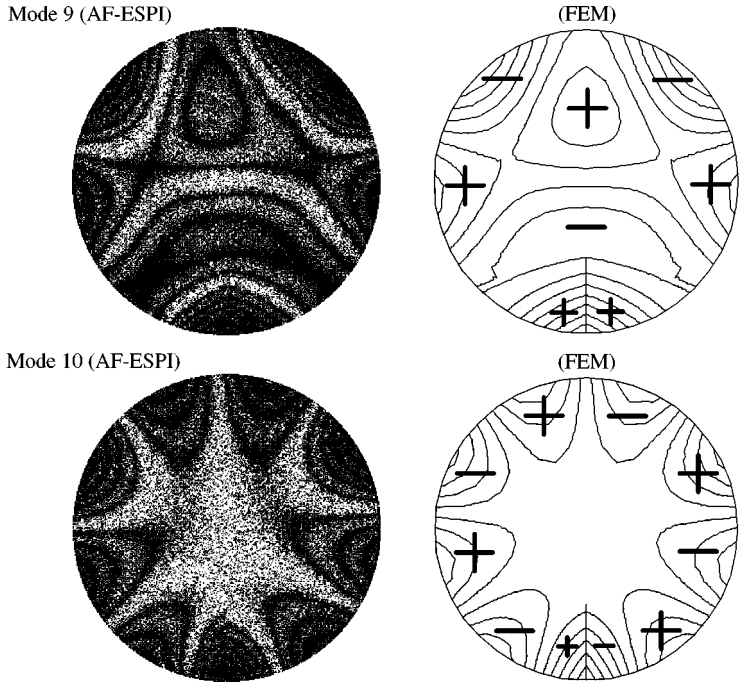

Figure 4. Continued.

4. CONCLUSIONS

It has been shown that the optical ESPI method has the advantages of non-contact and full-field measurement, submicron sensitivity, validity of both static deformation and dynamic vibration, and direct digital image output. A self-arranged amplitude-fluctuation ESPI optical set-up with good visibility and noise reduction has been established in this study to obtain the resonant frequencies and the corresponding mode shapes of free vibrating cracked circular plate at the same time. Compared with the spectrum analysis or modal analysis method, AF-ESPI is more convenient in experimental operation. Numerical calculations of resonant frequencies and mode shapes based on a finite element package are also performed and good agreements are obtained when compared with experimental measurements. The influence of the crack length on the vibration behavior of the cracked circular plate is discussed in detail. The resonant frequencies for antisymmetric types decrease more violently than that for symmetric types as the crack length increases. However, the symmetric types almost maintain similar mode shapes and have small variation of resonant frequencies for different crack lengths. Finally, the displacement and COD along the crack face are also investigated. It is interesting to find that the displacements at some modes are completely in phase which makes zero COD (i.e., modes 2, 3, 5, 7 and 9 for the C20 plate; modes 2, 3, 5, 8 and 9 for the C50 plate), and the stress intensity factor will be zero which implies that we have no fracture problem at these resonant frequencies.

ACKNOWLEDGMENT

The authors gratefully acknowledge the financial support of this research by the National Science Council (Republic of China) under Grant NSC 88-2212-E002-046.

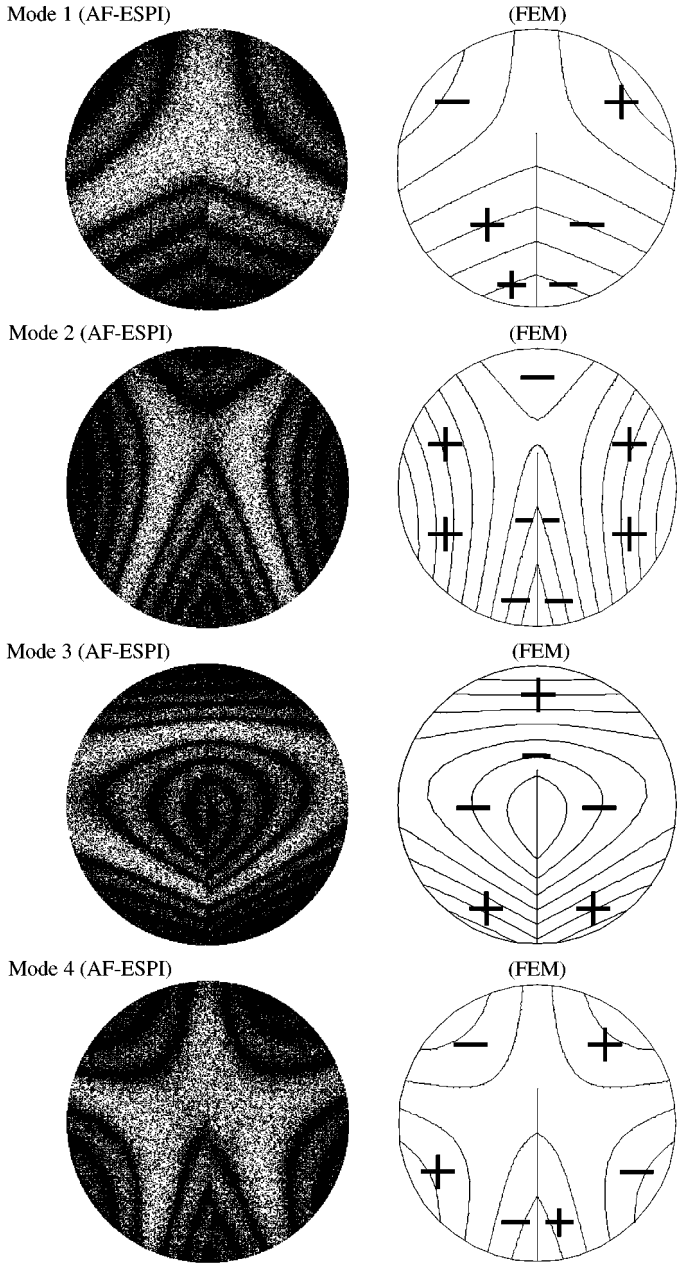

Figure 5. Mode shapes of the C50 plate obtained by AF-ESPI and FEM.

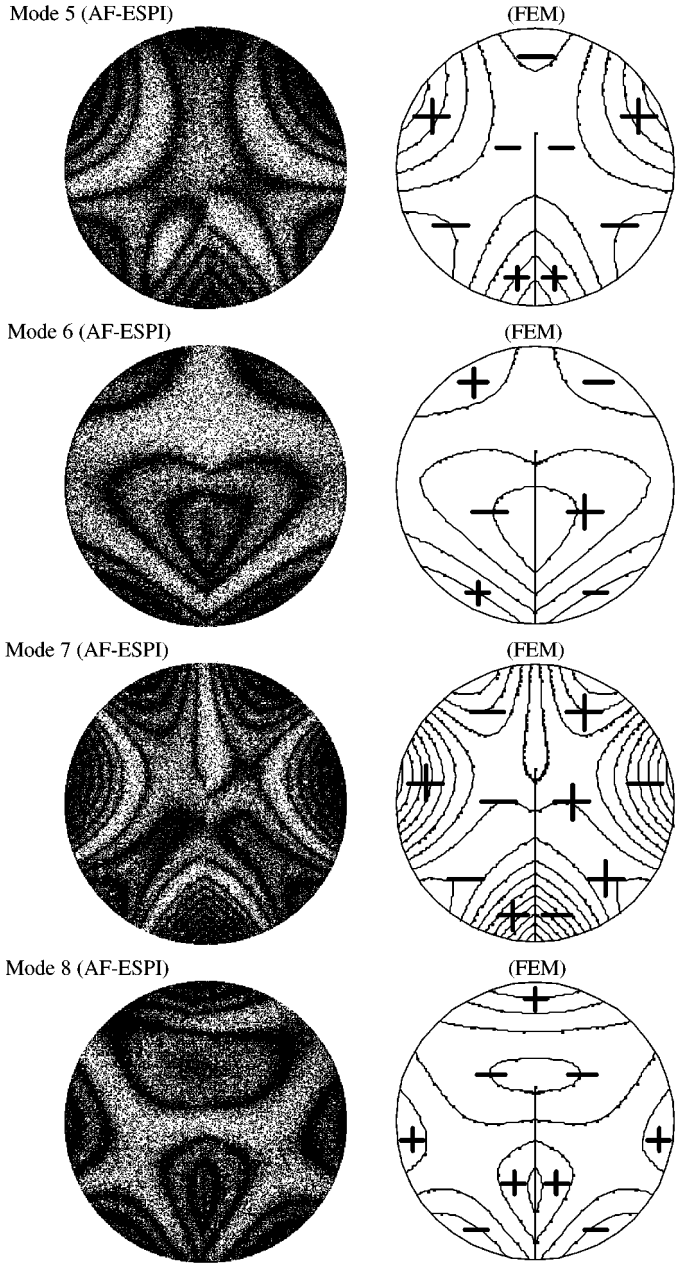

Figure 5. Continued.

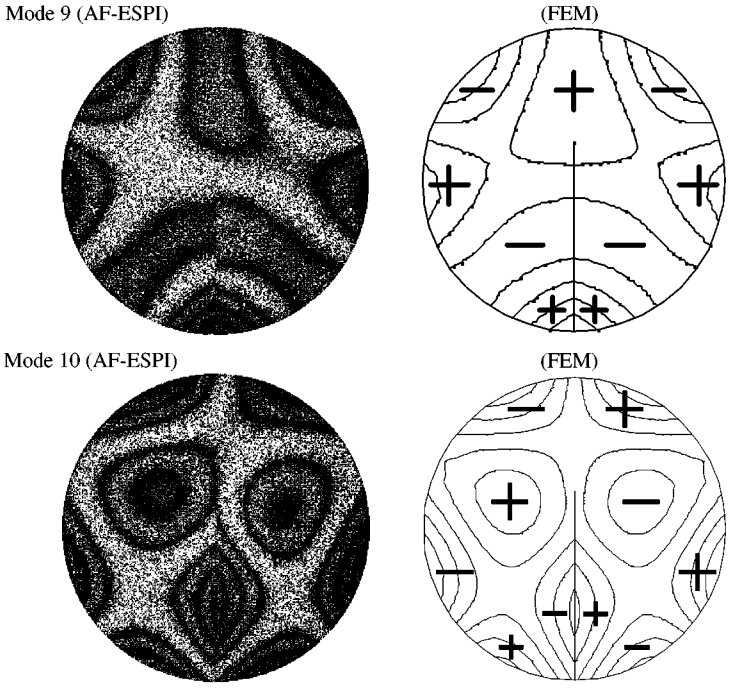

Figure 5. Continued.

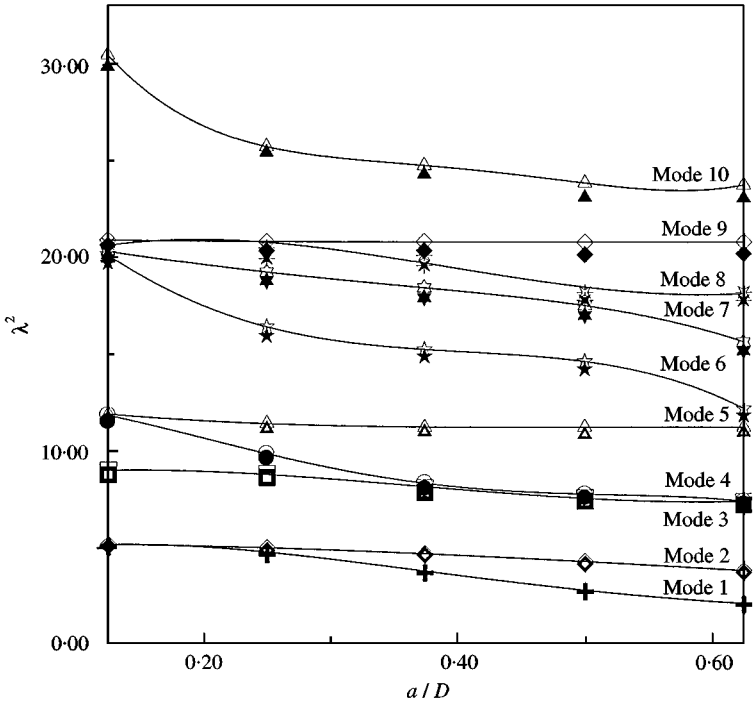

Figure 6. The resonant frequencies obtained from AF-ESPI and FEM for cracked circular plates with different crack lengths. ▲, experiment; △ FEM.

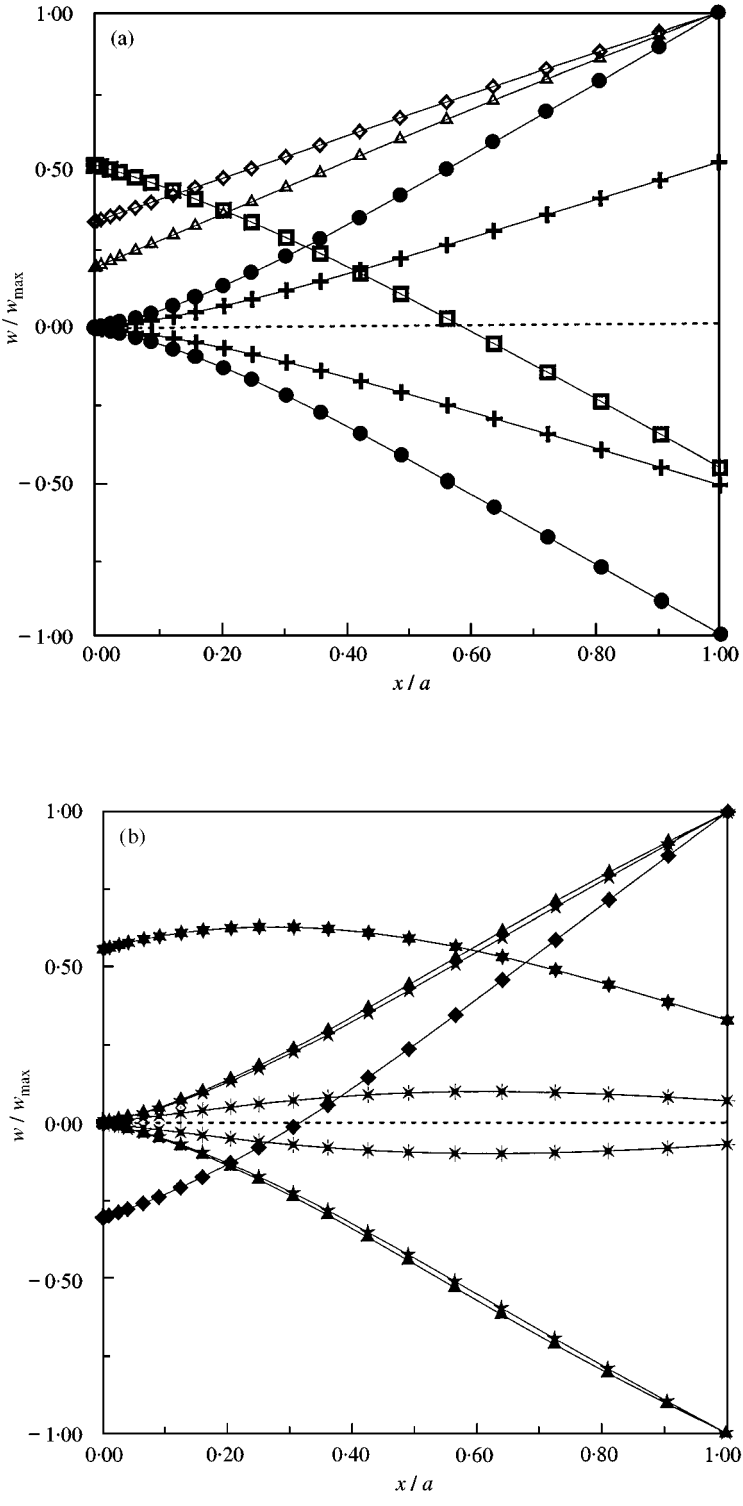

Figure 7. (a), (b) The normalized displacement (w/w_{max}) and (c) COD/w_{max} values of the crack faces for the C20 plate: —+— Mode 1; —◇— Mode 2; —□— Mode 3; —●— Mode 4; —△— Mode 5; —★— Mode 6; —✲— Mode 7; —*— Mode 8; —◆— Mode 9; —▲— Mode 10.

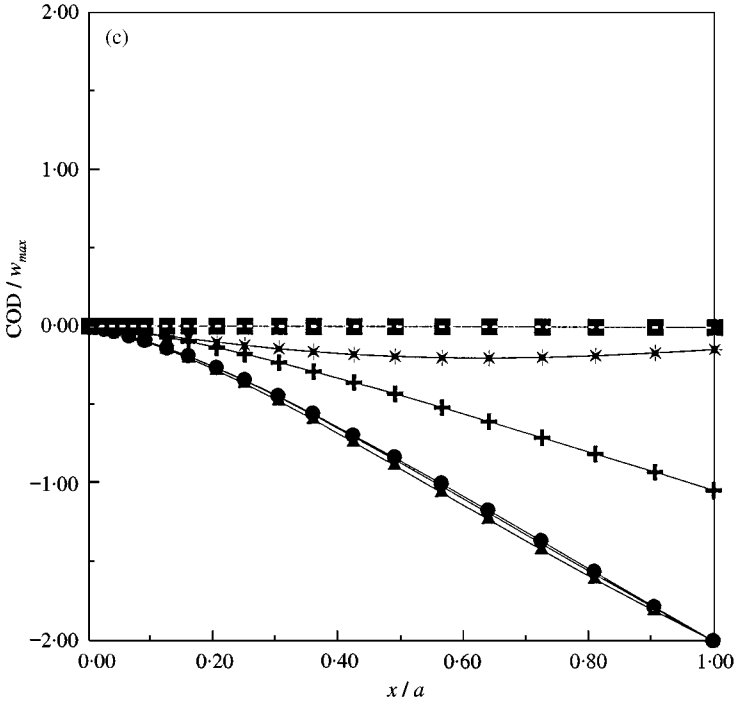

Figure 7. Continued.

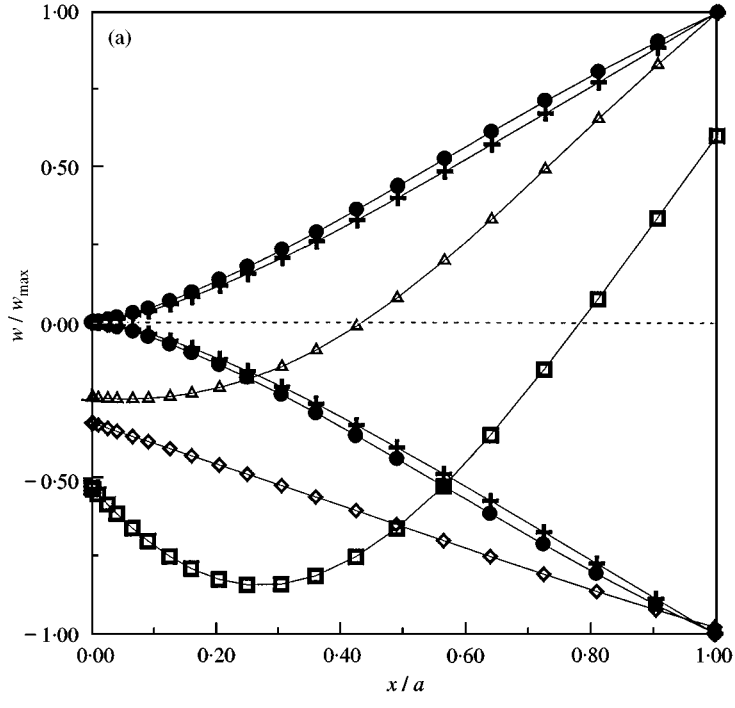

Figure 8. (a), (b) The normalized displacement (w/w_{max}) and (c) COD/w_{max} values of the crack faces for the C50 plate: —+— Mode 1; —◇— Mode 2; —□— Mode 3; —●— Mode 4; —△— Mode 5; —★— Mode 6; —✲— Mode 7; —*— Mode 8; —◆— Mode 9; —▲— Mode 10.

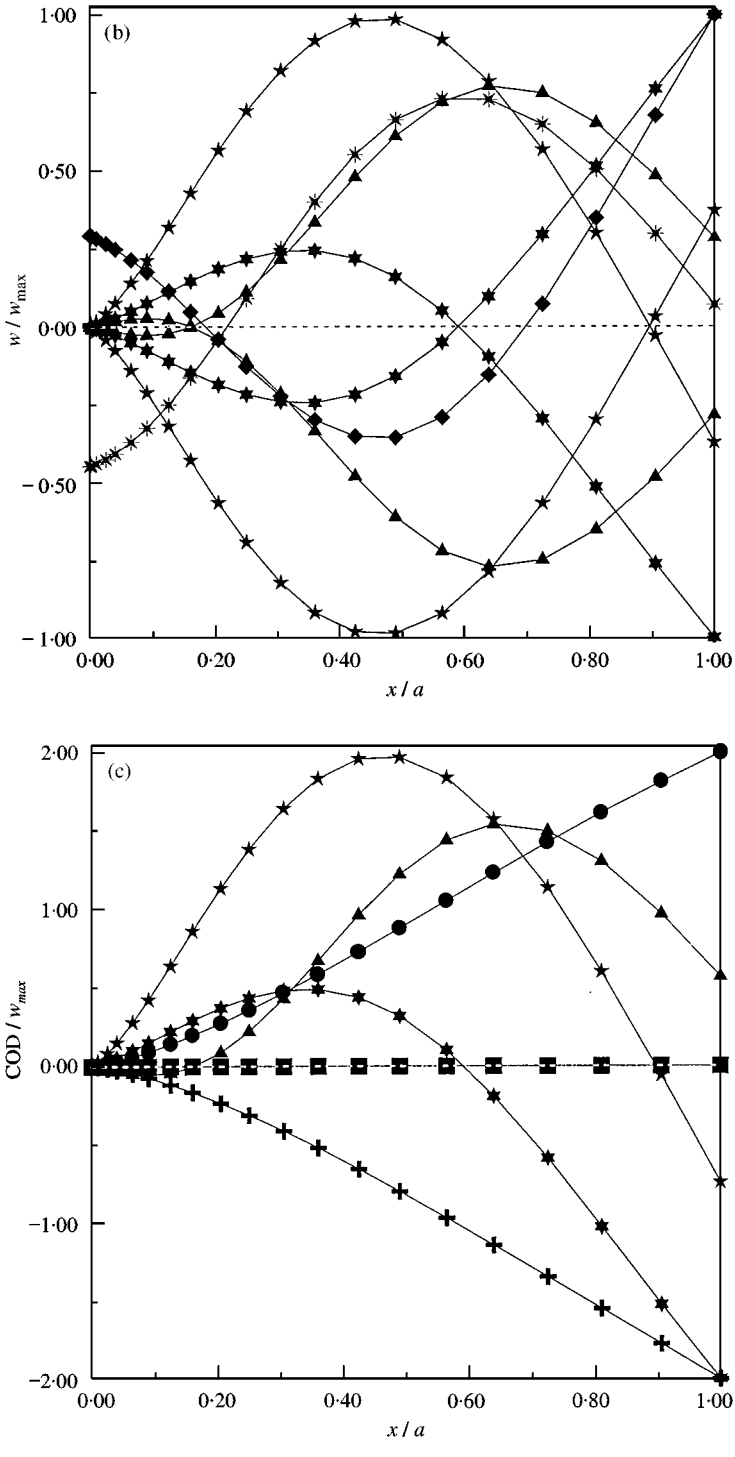

Figure 8. Continued.

REFERENCES

1. J. N. Butters and J. A. Leendertz 1971 *Optics and Laser Technology* **3**, 26–30. Speckle pattern and holographic techniques in engineering metrology.
2. P. K. Rastogi 1994 *Holographic Interferometry*, Berlin: Springer-Verlag.
3. R. Jones and C. Wykes 1989 *Holographic and Speckle Interferometry*. Cambridge: Cambridge University Press.
4. O. J. Løkberg and K. Hogmoen 1976 *Journal of Physics E*: *Scientific Instruments* **9**, 847–851. Use of modulated reference wave in electronic speckle pattern interferometry.
5. A. P. M. Hurden 1982 *NDT International* **15**, 143–148. An instrument for vibration mode analysis using electronic speckle pattern interferometry.
6. M. C. Shellabear and J. R. Tyrer 1991 *Optics and Lasers in Engineering* **15**, 43–56. Application of ESPI to three-dimensional vibration measurements.
7. K. Creath and G. Å. Slettemoen 1985 *Journal of the Optical Society of America. A* **2**, 1629–1636. Vibration-observation techniques for digital speckle-pattern interferometry
8. B. Pouet, T. Chatters and S. Krishnaswamy 1993 *Journal of Nondestructive Evaluation* **12**, 133–138. Synchronized reference updating technique for electronic speckle interferometry.
9. W. C. Wang, C. H. Hwang and S. Y. Lin 1996 *Applied Optics* **35**, 4502–4509. Vibration measurement by the time-averaged electronic speckle pattern interferometry.
10. C. C. Ma and C. H. Huang 2000 *IEEE Transactions on Ultrasonics*, *Ferroelectrics*, *and Frequency Control*. The investigation of three-dimensional vibration for piezoelectric rectangular parallelepipeds by using the AF-ESPI method (accepted).
11. C. H. Huang and C. C. Ma 1998 *AIAA Journal* **36**, 2262–2268. Vibration characteristics for piezoelectric cylinders using amplitude-fluctuation electronic speckle pattern interferometry.
12. S. D. Poisson 1829 *Memoires de L'Academie Royale des Sciences de L'Institute de France*, **8**, 357–570. L'Equilibre et le mouvement des corps elastiques.
13. A. W. Leissa 1969 *Vibration of Plates*, *NASA SP*-160. Washington, D.C.: U. S. Government Printing Offices.
14. R. John and M. A. Airey 1911 *Proceeding of the Physical Society of London* **23**, 225–232. The vibration of circular plates and their relation to Bessel functions.
15. T. Wah 1962 *The Journal of the Acoustical Society of America* **34**, 275–281. Vibration of circular plates.
16. W. Eversman and R. O. Dodson Jr. 1969 *AIAA Journal* **7**, 2010–2012. Free vibration of a centrally clamped spinning circular disk.
17. K. Itao and S. H. Crandall 1979 *Journal of Applied Mechanics* **46**, 448–453. Natural modes and natural frequencies of uniform, circular, free–free plates.
18. T. Irie, G. Yamada and S. Aomura 1980 *Journal of Applied Mechanics* **47**, 652–655. Natural frequencies of Mindlin circular plates.
19. Y. Stavsky and R. Loewy 1971 *The Journal of the Acoustical Society of America* **49**, 1542–1550. Axisymmetric vibrations of isotropic composite circular plates.
20. V. Marchand, J. Authesserre, J. Pouyet and C. Bacon 1996 *Journal of Sound and Vibration* **194**, 497–512. Determination of the elastic constants of materials, in the form of plates, by a free vibration method.
21. A. W. Leissa 1977 *The Shock and Vibration Digest* **9**, 13–24. Recent research in plate vibration: classical theory.
22. A. W. Leissa 1981 *The Shock and Vibration Digest* **13**, 11–22. Plate vibration research, 1976–1980: classical theory.
23. A. W. Leissa 1987 *The Shock and Vibration Digest* **19**, 11–18. Recent studies in plate vibration: 1981–85, part 1, classical theory.
24. A. W. Leissa, O. G. McGee and C. S. Huang 1993 *Journal of Sound and Vibration* **161**, 227–239. Vibration of circular plates having V-notches or sharp radial cracks.
25. O. G. McGee, A. W. Leissa, C. S. Huang and J. W. Kim 1995 *Journal of Sound and Vibration* **181**, 185–201. Vibration of circular plates with clamped V-notches or rigidly constrained radial cracks.
26. K. Ramesh, D. P. S. Chauhan and A. K. Mallik 1997 *Journal of Sound and Vibration* **206**, 266–274. Free vibration of an annular plate with periodic radial cracks.
27. *ABAQUS User's Manual*, *Version* 5.5. 1995 Rhode Island: Hibbitt, Karlsson and Sorensen, Inc.